Journal of Power Sources 196 (2011) 3933–3941

Contents lists available at ScienceDirect

Journal of Power Sources

journal homepage: www.elsevier.com/locate/jpowsour

A nonlinear viscoelastic–viscoplastic constitutive model for ionomer membranes in polymer electrolyte membrane fuel cells

Wonseok Yoon [a], Xinyu Huang [b,*]

[a] Florida Solar Energy Center and Department of Mechanical, Materials, and Aerospace Engineering, University of Central Florida, 1679 Clearlake Rd., Cocoa, FL 32922-5703, United States

[b] Mechanical Engineering Department and SOFC Program, College of Engineering and Computing, University of South Carolina, 300 Main Street, Columbia, SC 29208, United States

ARTICLE INFO

Article history:
Received 11 October 2010
Received in revised form
14 December 2010
Accepted 14 December 2010
Available online 21 December 2010

Keywords:
PEMFC
Nafion
Ionomer membrane
Viscoelastic
Viscoplastic
Constitutive model

ABSTRACT

This paper describes a phenomenological constitutive model for ionomer membranes in polymer electrolyte membrane fuel cells (PEMFCs). Unlike the existing approaches of elasto-plastic, viscoelastic, and viscoplastic model, the proposed model was inspired by micromechanisms of polymer deformation. The constitutive model is a combination of the nonlinear visco-elastic Bergström–Boyce model and hydration–temperature-dependent empirical equations for elastic modulus of ionomer membranes. Experiment results obtained from an uniaxial tension test for Nafion NR-111 membrane under well controlled environments were compared with simulated results by the finite element method (FEM) and the proposed model showed fairly good predictive capabilities for the large deformation behavior of the Nafion membrane subjected to the uniaxial loading condition in a wide range of relative humidity and temperature levels including liquid water.

1. Introduction

Mechanical behavior of polymer electrolyte membrane (PEM) has been studied over a wide range of temperature and relative humidity (RH) conditions by many research groups due to the significance of the membrane durability in fuel cell operation [1–9]. Perfluorosulfonic acid (PFSA) membrane, originally developed by DuPont with the trade name Nafion®, is widely used in the PEM fuel cell. It is believed that membrane failure is the major fuel cell life determining factor [10,11]. PFSA membrane can absorb water and undergoes microstructure transformation, primarily the formation of hydrophilic ionic clusters in hydrophobic perfluorinated ionomers matrix. This imparts the membrane proton conductivity; it also causes the mechanical property of ionomer membrane to vary with respect to temperature and hydration level. At low temperature below 90 °C, water acts as plasticizer softening the membrane and reducing load carrying capability. However, at elevated temperature above 90 °C surprisingly, the opposite trend is observed; the more water a membrane absorbs, the stronger the membrane becomes [3,5,8]. This abnormal behavior was attributed to change in viscoelastic response of Nafion due to microphase structural transitions driven by changes in temperature and water activity [5].

It is very important to know the maximum level of membrane stress when designing a fuel cell device. Stress distribution in the membrane is also important for the understanding of the membrane degradation mechanisms. The authors recently investigated the mechanical stress effect on chemical degradation of ionomer membrane and found that the mechanical stress accelerates the rate chemical decomposition of the PEM by oxygen radical attacks [10]. Direct measurement of membrane stress in fuel cells is not always possible; using numerical models to predict mechanical stress in the ionomer membrane in various conditions in fuel cells is often the only choice. The macromolecular nature of polymer is characterized by the covalently bonded and long chain structure [12]. The physical properties of polymeric systems are strongly affected by chain microstructure, i.e., isomerism, which is the organization of atoms along the chain as well as the chemical identity of monomer units [13]. An important feature controlling the properties of polymeric materials is polymer architecture. The Nafion® membrane is a copolymer containing at least two monomers, i.e., a TFE backbone and perfluoro(4-methyl-3, 6-dioxa-7-octene-1-sulfonyl fluoride) [14]. A large amount of polymer research works continue to be directed towards the study of molecular mechanisms

* Corresponding author. Tel.: +1 803 777 6834; fax: +1 803 777 0106.
E-mail address: huangxin@cec.sc.edu (X. Huang).

0378-7753/$ – see front matter © 2010 Elsevier B.V. All rights reserved.
doi:10.1016/j.jpowsour.2010.12.034

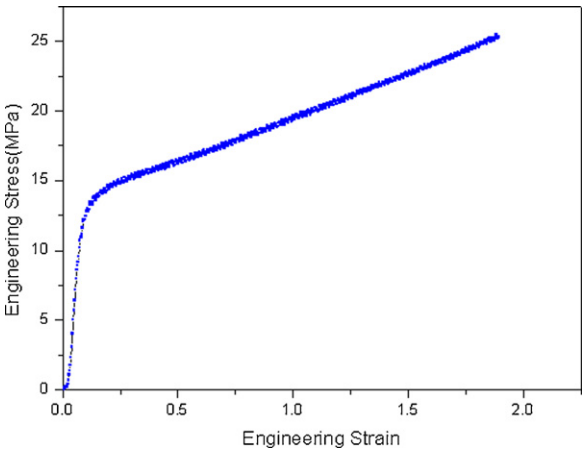

Fig. 1. Tensile stress–strain curve of Nafion NRE 212 tested at room temperature with 4.2 mm s^{-1} pulling rate.

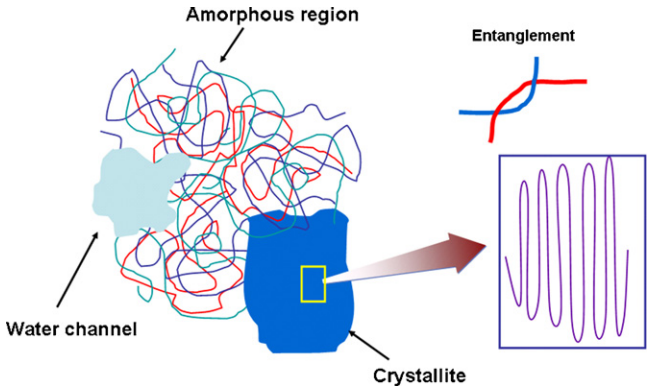

Fig. 2. Schematic of hierarchy of ionomer membrane structure

governing their structure–property relationships. Among them, the stress–strain response of polymers has been recognized for a long time as one of the most informative properties [15]. Fig. 1 shows the typical stress–strain curve for a Nafion NRE-212 membrane. Macroscopic nature of the mechanical behavior for the Nafion® membrane under the tensile stress before rupture is characterized by an elastic response (Hook's law), followed by the strain hardening in the plastic deformation range after the yield point. These elastic and plastic deformation for the membrane is also time-dependent, i.e., visco-elastic and visco-plastic. Experimental data presented in the Solasi's work [16] clearly demonstrated the complicated non-linear time–, hydration-level-, and temperature-dependent behavior of the ionomer membrane.

It is assumed that when an external load is applied to a polymer, the molecular bonds experience stress, and in order to relieve themselves as much as possible, the chain segments undergo internal rearrangements [15]; the way the polymer reacts to the external stress is dependent on the magnitude and rate of the applied stress, chain morphology, environmental factors such as relative humidity (RH) and temperature. In literatures, it is believed that the Nafion® membrane consists of at least two phases [17]; an amorphous phase and a crystalline phase, and the crystallinity for 1100 EW membrane is in a range between 5 and 20% [18]. Therefore, it is expected that each component contributes to the deformation resistance differently.

Haward and Thackray [19] attempted to interpret this macroscopic constitutive behavior of polymer based on the microstructure of polymers. The polymer's mechanical response was described by with two parallel processes as the initial non-linear elastic response controlled by the secondary intermolecular interactions, and the entanglement network response controlled by the primary intramolecular interactions which give an entropic contribution at large strains. As a continuous attempt for describing the mechanical behavior of polymers, specifically, ionomer membrane, we propose a nonlinear visco-elastic–visco-plastic constitutive model by introducing hydration dependence into Bergström and Boyce's model [20] published in 1998.

2. Constitutive modeling of ionomer membrane

2.1. Micro-mechanism of polymer deformation

The constitutive model of ionomer membranes is needed for continuum mechanics model to predict the distribution of the stress and strain in the fuel cell membrane. The typical stress–strain behavior in Fig. 1 can be qualitatively described by the initial Hookean elasticity until the stress developed becomes sufficiently large to produce a plastic deformation at the imposed rate. Following a strain hardening region after the yield point, the deformation eventually leads to the final rupture of the membrane; it is generally believed that the rupture of the polymer is induced by a defect (microcracks, crazing) formation and accumulation process [21,22]. To model the mechanical behavior of the polymer membrane subjected to uniaxial stretching, researchers have applied linear elasticity [23], visco-plasticity [24], and elasto-plastic theory [1,6,25]. None of the models can account for the effects of all known micro-mechanisms of the ionomer deformation, such as a reptational plastic flow, chain entanglement, and entropic effect on deformation.

Fig. 2 shows a hypothetical hierarchical structure of the ionomer membrane consisting of the amorphous network, crystalline regions, and water clusters. It has been established by many investigators that molecular chain orientation evolves with magnitude and state of strain to produce strain hardening in polymers [26,27] and the polymer macromolecular structure, which forms a network by virtue of physically entangled molecular chains, evolves during deformation as secondary valence interactions dissociate with plastic strain [28]. Entanglements, a topological constraint, develop from the interpenetration of random-coil chains and are of importance in determining rheological, dynamic, and fracture properties [29,30].

Chain mobility and morphological relaxation of intermolecular chain are expected to increase with temperature, which can be explained by reptational dynamics [31]. Also, it is reported that the mechanical stress increases the molecular mobility during plastic deformation [32].

Considering the characteristic morphology and microstructure of the ionomer membrane reported by a number of researches [15,33,34], the mechanical deformation mechanisms of the PFSA based ionomer are hypothesized as follows:

1. The physical crosslinks formed by molecular entanglements, ionic interaction in sulfonic acid groups and intermolecular, secondary (Van der Waals) interactions in crystalline phase bears the low stresses in the elastic region of the stress–strain curve, leaving the major portion of covalent bonds unaffected.
2. When the external load is increased beyond a certain level, ionic domains start to permanently deform, elongate and reorient [34]; as the stress develop, some chains in the amorphous and/or crystalline phase can overcome the secondary interactions and develop irreversible slippage and reorientation, yielding occurs. As stress/strain increases further, the perma-

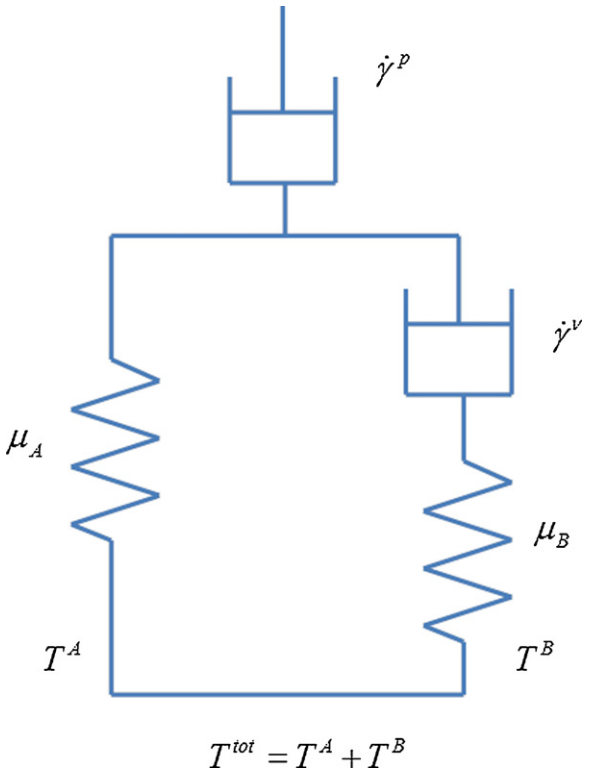

Fig. 3. One dimensional rheological representation of the constitutive model for the ionomer membrane.

nently entangled chains (which can not slip out of physical entanglements) become taut and start locking up, resulting in strain hardening. As strain increases further, small crystallites can disintegrate [33].

Based on the hypothesized deformation micro-mechanisms for the ionomer membrane, a 1D rheological representation of the constitutive model (as shown in Fig. 3) is proposed. The mechanical behavior for ionomer membranes can be decomposed into two parts: a visco-plastic response, which is relevant to irreversible molecular chain slippage and a time-dependent viscoelastic response. The viscoelastic response can be further decomposed into the response of two molecular networks acting in parallel: a first network (A) represents the equilibrium of the visco-elastic response and a second network (B) the time-dependent deviation from the visco-elastic equilibrium state. This idea, called Dual Network Fluoropolymer (DNF) model, was initially developed by Bergström for modeling fluoropolymers [35]. The decomposition idea was also used by Boyce [36] and Bergström [37,38]. The Cauchy stress acting on the network A and B can be modeled by any of the classical nonlinear hyper-elasticity models for elastomers. In this research, the Cauchy stress which is a function of the Cauchy–Green deformation tensor followed that of the Bergström and Boyce's model [20] for elastomers, which is based on the eight-chain model of Arruda and Boyce [26]. Also, the plastic flow rule for the network B is motivated by reptational dynamics of a polymer [31,39]. The DNF model does not account for the hydration effect on the mechanical properties of ionomer membranes originated from the water containing ionic clusters formed by sulfonic acid groups. For the modeling of ionomer membranes, it is assumed that hydration effect can be incorporated implicitly into the empirical equation for the elastic modulus, which is explained in details in the modeling section below.

2.2. Constitutive modeling

For the analysis of the large deformation of polymers, the concept of multiplicative decomposition of the deformation gradient into elastic and plastic parts had been typically employed instead of an additive decomposition [27,36–38,40–44]. The mathematical description of the constitutive model for ionomer membranes is based on the breakdown of the overall deformation into the visco-elastic and visco-plastic deformation which is referred to as the Kröner–Lee decomposition. The deformation gradient F can be expressed by Eq. (1), as shown below [35]:

$$F = F^{ve}F^{p} \tag{1}$$

F^p is the deformation due to pure plastic flow representing irreversible chain motion, and $F^{ve} = F^A = F^B$ is the remaining contribution to F associated with distortion and reorientation of crystallites and entanglement of polymer chains.

The visco-elastic deformation gradient is further decomposed into elastic and viscous parts:

$$F^{ve} = F^{e}F^{v} \tag{2}$$

Here, F^e is the reversible (elastic) deformation gradient and F^v indicates the viscous deformation gradient. The spatial velocity gradient L is given by $L = \dot{F}\cdot F^{-1}$. By inserting $F = F^{ve}F^{p}$ into $L = \dot{F}\cdot F^{-1}$, the corresponding rate kinematics can be decomposed into visco-elastic and visco-plastic contributions as well:

$$L = \dot{F}\cdot F^{-1} = (\dot{F}^{ve}F^{p} + F^{ve}\dot{F}^{p})(F^{ve}F^{p})^{-1} = L^{ve} + \tilde{L}^{p} \tag{3}$$

Here, $\tilde{L}^p = \tilde{D}^p + \tilde{W}^p$ can be described as the sum of the symmetric (the rate of deformation, $\tilde{D}^p$) and the skew-symmetric part (the spin tensors, $\tilde{W}^p$.) Similarly, the velocity gradient of viscoelastic parts can be decomposed into elastic and viscous components: $L^{ve} = \dot{F}^{ve}\cdot F^{ve^{-1}} = L^e + \tilde{L}^v$, where $\tilde{L}^v = \tilde{D}^v + \tilde{W}^v$. The intermediate configurations described by p and v, in general, cannot be uniquely determined, since an arbitrary rigid rotation can be superimposed on it and leave it stress free [45]. The intermediate state can be determined uniquely in different ways and one convenient way is to prescribe $\tilde{W}^v = 0$ and $\tilde{W}^p = 0$, which means that the flow is irrotational [46]. In addition to that, plastic and viscous deformation are assumed to be incompressible, i.e., $\det(F^v) = 1$ and $\det(F^p) = 1$. In our study, the volumetric swelling and shrinkage behavior of the Nafion as functions of the hydration level and temperature are not considered in the kinematics during the deformation, the hydration level and temperature are assumed to be constants in a given loading condition. Also, the deformation of Nafion over whole strain range is assumed to be nearly incompressible, $\det(F) \approx 1$ as well.

The Cauchy stress tensor for network A is given by the eight-chain representation [26,37]:

$$T^A = f_{8ch}(F^{ve}) = \frac{\mu_A}{J^{ve}\overline{\lambda^{ve}}}\cdot\frac{L^{-1}(\overline{\lambda^{ve}}/\lambda^{lock})}{L^{-1}(1/\lambda^{lock})}\mathrm{dev}\,[\mathbf{B}^{ve*}] + \kappa[J^{ve} - 1]1 \tag{4}$$

where $J^{ve} = \det[F^{ve}]$, μ_A is a temperature and hydration level dependent initial shear modulus, λ^{lock} is the chain locking stretch, $\mathbf{B}^{ve*} = (J^{ve})^{-2/3}F^{ve}(F^{ve})^{T}$ is the left Cauchy Green tensor, $\overline{\lambda^{ve}} = \sqrt{tr(\mathbf{B}^{ve*})/3}$ is the effective chain stretch based on the eight-chain assumption, $L^{-1}(x)$ is the inverse Langevin function, where $L(x) = \coth(x) - 1/x$, and κ is the bulk modulus. To obtain the inverse, a curve fit of the inverse Langevin function is used for all x as follows [39]:

$$L^{-1}(x) \approx \begin{cases} 1.31446\tan(1.58986x) + 0.91209x, & \text{if } |x| < 0.84136 \\ 1/(\mathrm{sign}(x) - x) & \text{if } 0.84136 \le |x| \le 1 \end{cases} \tag{5}$$

The Cauchy stress tensor for network B can be calculated from the same eight-chain representation that was used for network A and computed by multiplication the eight-chain expression on the elastic deformation gradient F^e with a scalar factor s_B which can be

Table 1
Fitting constants for elastic modulus equation.

A_1	B_1	A_2	B_2
0.000645	−0.058673	−0.014673	10.534189

considered as a specific material parameter.

$$T^B = s_B \cdot f_{8ch}(F^e) = s_B \cdot \left(\frac{\mu_B}{J^e \overline{\lambda^e}} \cdot \frac{L^{-1}(\overline{\lambda^e}/\lambda^{lock})}{L^{-1}(1/\lambda^{lock})} \mathrm{dev}\,[\mathbf{B}^{e*}] + \kappa[J^e - 1]1 \right) \tag{6}$$

Then, the total Cauchy stress can be calculated as the sum of the two resultants, $T = T^A + T^B$. The First Piolar Kirchhoff stress, P which relates forces in the present configuration with areas in the reference configuration can be calculated from conversion between two stress, $P = J \cdot T \cdot F^{-T} = J \cdot (T^A + T^B) \cdot F^{-T}$. In order to incorporate the hydration- and temperature-dependent mechanical property such as μ_A and μ_B for ionomer membranes, empirical relationship of elastic modulus as a function of membrane water content, λ_m and temperature, θ (°C) was used. The bulk modulus κ is assumed to be a constant and its magnitude was taken as a reasonable value in the analysis. It was found that the simulated stress is not significantly affected by the bulk modulus. Earlier attempt for the empirical relation of the elastic modulus was made by Hsu et al. [47]. In [48], the uniaxial testing data for N111 membrane were collected under controlled temperature and RH environments and these data sets were used for fitting the exponential type function as shown below:

$$E(\lambda, \theta) = \exp\{(A_1 \cdot \theta + B_1) \cdot \lambda_m + (A_2 \cdot \theta + B_2)\} \tag{7}$$

where $\lambda_m = 0.043 + 17.81 a_T - 39.85 a_T^2 + 36.0 a_T^3 \quad \text{for } 0 < a_T \le 1$ [49] and a_T is the water activity (RH) defined by $a_T = p_w / p_{sat}(\theta)$, where p_w is water vapor pressure and p_{sat} is saturation water vapor pressure at the temperature. From the elastic modulus equation, the initial shear modulus for network A and B can be described by

$$\mu_B = s_{0B} \cdot E(\lambda, \theta) = s_{0B} \cdot \exp\{(A_1 \cdot \theta + B_1) \cdot \lambda_m + (A_2 \cdot \theta + B_2)\} \tag{8}$$

$$\mu_A = s_{0A} \cdot \mu_B \tag{9}$$

where s_{0A} and s_{0B} are material parameters and A_1, B_1, A_2, and B_2 are fitting constants listed in Table 1.

The rate of visco-plastic flow of network B can be described by $\tilde{D}^v = \dot{\gamma}^v N^v$. The tensor N^v specifies the directions of the driving stresses of the relaxed configuration convected to the current configuration, and the terms $\dot{\gamma}^v$ indicates the flow rates being given by the reptation-inspired equation [37]:

$$\dot{\gamma}^v = \dot{\gamma}_0 [\overline{\lambda}^v - 1]^c \cdot \left(\frac{\tau^e}{\tau_{base} + \beta p^e} \right)^m \cdot \left(\frac{\theta}{\theta_{base}} \right)^n \tag{10}$$

where $\tau^e = \left\| \mathbf{T}^{e'} \right\|_F \equiv (tr[\mathbf{T}^{e'} \mathbf{T}^{e'}])^{1/2}$ is the Frobenius norm of $\mathbf{T}^{e'} = \mathrm{dev}\,[\mathbf{T}^e]$, the direction of the driving stress is described by $N^v = \mathbf{T}^{e'}/\tau^e$, $\overline{\lambda}^v = \sqrt{tr(\mathbf{B}^{v*})/3}$ is an effective viscous chain stretch, $\mathbf{B}^{v*} = (J^v)^{-2/3} F^v (F^v)^{\mathbf{T}}$ is the left Cauchy-Green deformation tensor, $p^e = -(T^e_{11} + T^e_{22} + T^e_{33})/3$ is the hydrostatic pressure, and $C \in [-1, 0]$, $m > 0$, n, β, $\dot{\gamma}_0$, θ_{base} and τ_{base} are material parameters. As pointed out by Bergström, the term $[\overline{\lambda}^v - 1]^c$ captures a strain-dependence of the effective viscosity and this might cause the term to grow numerically very large if the effective stretch $\overline{\lambda}^v$ is unity or close to unity in both the unloaded state and when the applied strain switches between tension and compression. One way to resolve this problem is to introduce a parameter $\varepsilon \approx 0.01$ to avoid the singularity and Eq. (10) can be modified as follows:

$$\dot{\gamma}^v = \dot{\gamma}_0 [\overline{\lambda}^v - 1 + \varepsilon]^c \cdot \left(\frac{\tau^e}{\tau_{base} + \beta p^e} \right)^m \cdot \left(\frac{\theta}{\theta_{base}} \right)^n \tag{11}$$

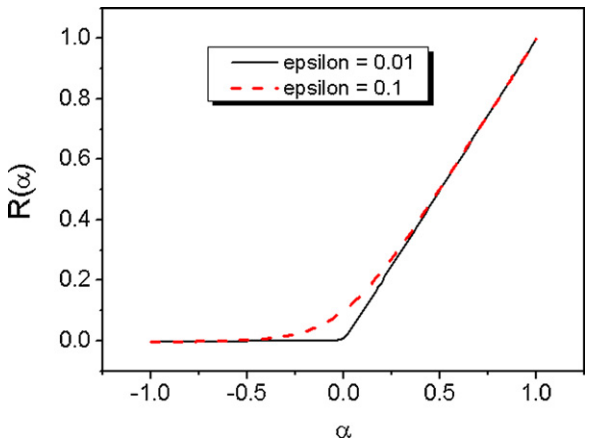

Fig. 4. Smooth ramp function.

As reported in [50], another way to eliminate the numerical difficulty is to use certain differentiable smooth ramp function $R(\alpha)$ (shown in Fig. 4.) which replaces $[\overline{\lambda}^v - 1]$ by $R(\overline{\lambda}^v - 1)$

where,

$$R(\alpha) = 2.8853 \cdot \varepsilon \cdot \left(0.3466 + 0.1733 \frac{\alpha}{\varepsilon} - 0.5 \cdot \ln \left\{ \frac{1}{\cosh[0.3446 \cdot (\alpha/\varepsilon)]} \right\} \right) \tag{12}$$

satisfying

$$\lim_{\alpha \to -\infty} \left(\frac{dR(\alpha)}{d\alpha} \right) = 0, \quad R(0) = \varepsilon, \quad \lim_{\alpha \to +\infty} \left(\frac{dR(\alpha)}{d\alpha} \right) = 1.$$

As a result, the velocity gradient of the viscous flow can be expressed as:

$$\tilde{L}^v = F^e L^v F^{e^{-1}} = \tilde{D}^v = \dot{\gamma}^v \frac{\mathbf{T}^{e'}}{\tau^e}$$

$$\dot{F}^v = F^{e^{-1}} \left(\dot{\gamma}^v \frac{\mathbf{T}^{e'}}{\tau^e} \right) F^e F^v \tag{13}$$

The rate of plastic flow can be described by a phenomenological equation [35]:

$$\dot{\gamma}^p = \begin{cases} a\, b\, (\varepsilon - \varepsilon_0)^{b-1} \dot{\varepsilon} & \text{if } \tau > \sigma_0 \\ 0 & \text{otherwise,} \end{cases} \tag{14}$$

where, $a > 0$, $b > 0$ and $\sigma_0 > 0$ are material parameters, $\tau = \left\| \mathrm{dev}[\mathbf{T}] \right\|_F$ is the Frobenius norm of the deviatoric part of the Cauchy stress T, and ε_0 is the effective strain when τ is equal to σ_0; the effective strain can be calculated from $\varepsilon = \left\| \mathrm{E}_{\ln} \right\|_F$, where $E_{\ln} = \ln[V]$ and V is the left stretch tensor, and $\dot{\varepsilon}$ is the effective strain rate. For our research, ε_0 is considered as a constant and the engineering strain rate was used for $\dot{\varepsilon}$ for the simplicity since the plastic flow rate can be controlled by choosing the appropriate parameters, a and b. As can be noticed in Eq. (14), the plastic flow rate is a function of the strain rate and the magnitude of current strain.

In summary, the velocity gradient of the plastic flow can be expressed as:

$$\tilde{L}^p = F^{ve} L^p F^{ve^{-1}} = \tilde{D}^p = \dot{\gamma}^p \frac{\mathrm{dev}[\mathbf{T}]}{\tau}$$

$$\dot{F}^p = F^{ve^{-1}} \left(\dot{\gamma}^p \frac{\mathrm{dev}[\mathbf{T}]}{\tau} \right) F^{ve} F^p \tag{15}$$

3. Experimental

The experimental data of Nafion that we used to fit and verify the proposed model came from data reported in Yue Zou's thesis work

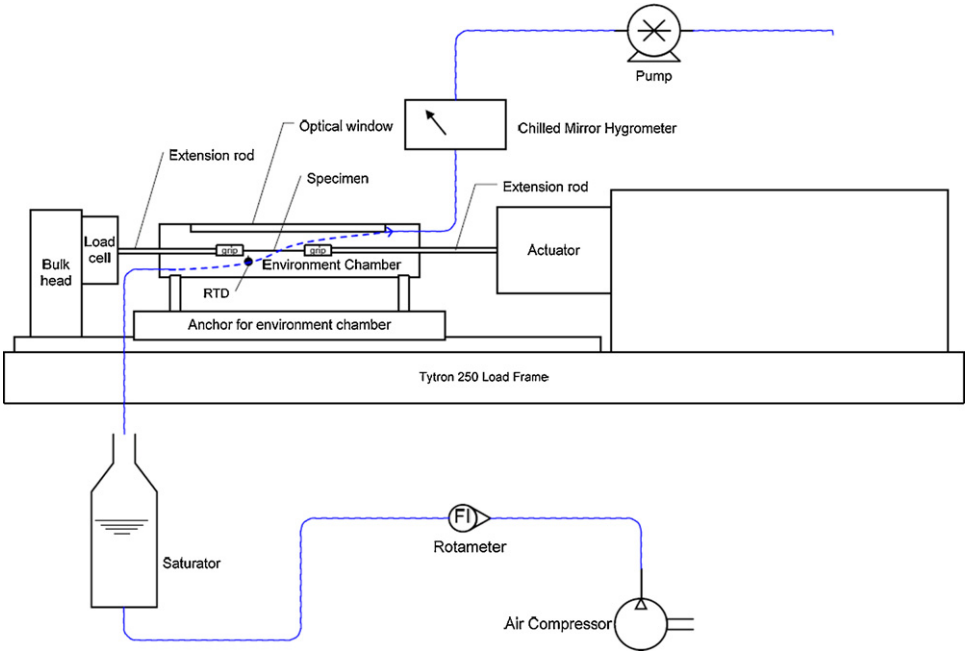

Fig. 5. Schematic diagram of membrane mechanical testing setup.

[48]. The mechanical test was performed on MTS Tytron^{TM} 250, a horizontal load frame designed especially for membrane testing. An environment chamber (T and RH) was built to fit the horizontal rail of Tytron load frame and the RH control was achieved by mixing dry and saturated gas stream. Steady-state RH values were taken from a chilled mirror dew point sensor (EdgeTech Dew Prime II) continuously sampling the RH of the gas existing the chamber and temperature was measured by a platinum RTD probe installed closely to the membrane sample inside the chamber. All the uniaxial tension tests data used in this study were conducted under environment with well-controlled relative humidity and temperature. The membrane samples, Nafion NR-111 (hereby referred to as N111 sample), were cut into rectangular shape with about 50 mm length and 6.5 mm wide. The specimens were equilibrated in the chamber for at least 1 h before the tests. Mechanical testing data at three different condition, which were 25 °C and 80%RH, 25 °C and 50%RH, and 65 °C and 75%RH were used for comparison with FEM results. The stress–strain curve for the samples is obtained by applying a tensile force at a uniform strain rate of 0.0132 s^{-1}.

To study the material properties in liquid water hydrated state, a water bath tray together with a U-type pulling rod were designed to perform tensile testing with the membrane sample fully immersed in water. The nominal cross-sectional area and gauge length of the specimens were used in the calculation of the engineering stress–strain curves from the displacement-load data for the vapor-equilibrated membrane and a linear expansion rate of 15% [51] were applied to compensate the volumetric expansion in the calculation of the cross-section area for the water-equilibrated membrane at 80 °C. The engineering stress and strain are converted to true stress and true strain when compared with the model prediction (Fig. 5).

4. Finite element simulation

The proposed constitutive model for ionomer membrane was implemented into Comsol Mutiphysics 3.5 software package. The Structure Mechanics and the PDE modules were utilized for the simulation of time dependent behavior of the membrane in an application module of plane stress. The PDE module was used for the integration of the time evolution equation for viscous flow and plastic flow. At every time step, the viscous and plastic deformation gradients were calculated and used for computing the Cauchy stress acting on the network A and B. To model the nearly incompressible material for ionomer membranes, mixed U–P formulation provided in the software was used for calculation of an independent variable, pressure p.

5. Results and discussion

Fig. 6(a) shows the engineering stress–strain curves of as received N111 membrane tested at three different environmental conditions and strain rates. Plastic deformation sets in at a strain around 0.1 and the material hardens along the rest of stress–strain curve. At large strain, the elastic component of the strain is negligible compared to the plastic strain. It can be seen that the elastic modulus and yield stress are decreasing with increasing temperature and RH. The slope of the strain-hardening portion of the stress–strain curve changes slightly with respect to temperature and humidity.

The stress–strain curves from FEM simulation (Fig. 6b–d) shows fairly good qualitative agreement with experimental behavior of vapor-equilibrated ionomer membranes. The FEM predicts temperature- and hydration-dependent mechanical behavior of membrane and the overall shape of the strain-hardening behavior matches the experiment results. The proposed constitutive model can accurately describe the mechanical behavior of the vapor-equilibrated membrane. Material parameters and other constants used at the simulation are tabulated in Tables 2 and 3.

From the rheological representation in Fig. 3, the true stress components can be dissociated into the stress acting on network A and network B. As mentioned earlier, the true stress from network A captures the equilibrium response of the material and network B represents time-dependent deviation from viscoelastic equilibrium state. As generally accepted, physical resistances which are related with intermolecular and intramolecular interactions govern the energy barrier that must be overcome to yield the material and to deform it up to large plastic strain [52]. These molecular

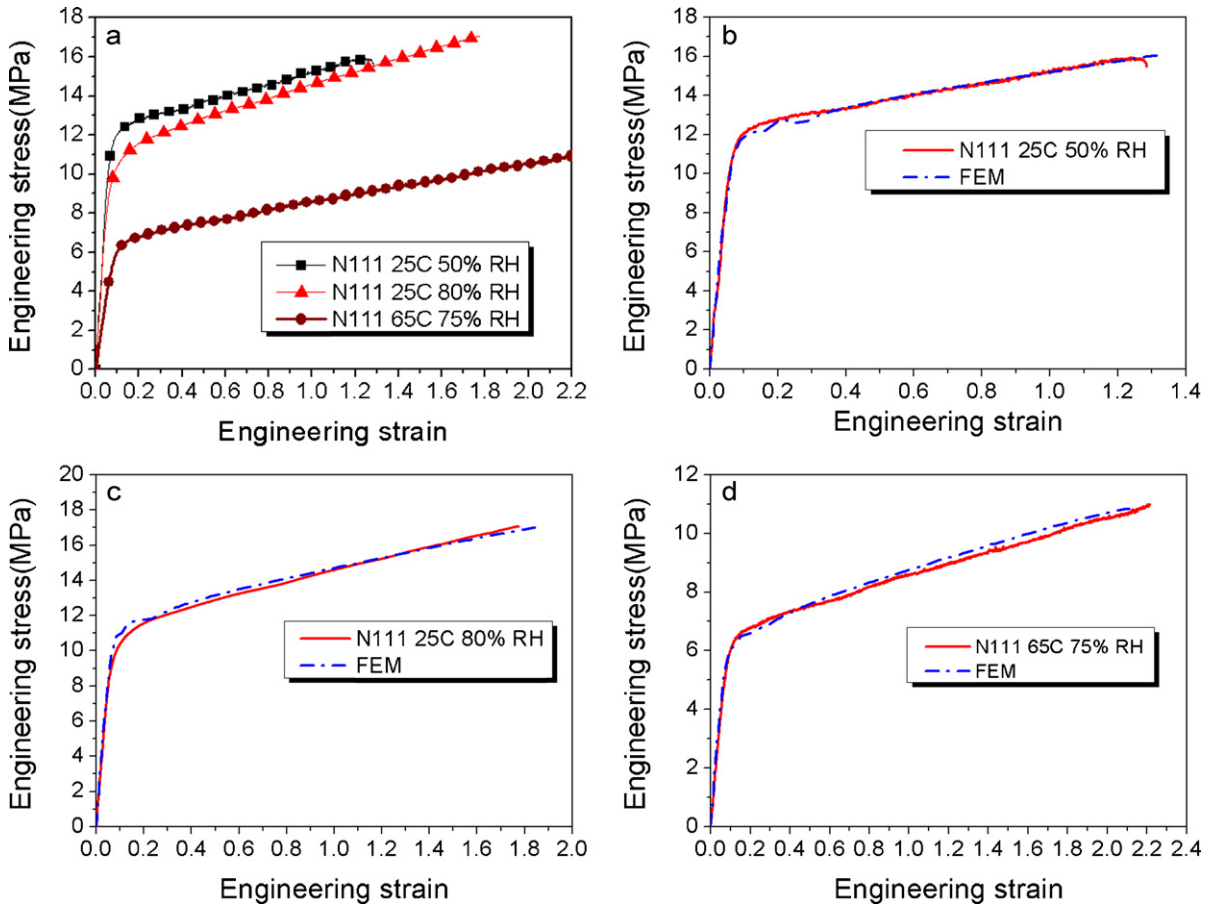

Fig. 6. (a) Experiment results of stress–strain curves of Nafion N111 membrane under the various test conditions, (b) FEM simulation results of N111 at 25 °C and 50%RH, (c) 25 °C and 80%RH, and (d) 65 °C and 75%RH.

Table 2
Material parameters used in the FEM simulation of vapor-equilibrated membranes.

C	−0.5
m	6
n	4.5
β	0.6
$\dot{\gamma}_0$	1
a	0.01
b	0.78
ε_0	0.01
σ_0	5 MPa
s_B	8
$\dot{\varepsilon}$	0.0132
θ_{base}	100
κ	97 MPa
λ_{lock}	6

interactions induce the rate and temperature effects prevailing in the material behavior.

Figs. 7 and 8 show the true stress components from the stress–strain curve calculated from FEM. At low strain, the stress is dominantly exerted by the intermolecular interactions (network B) in crystallites, amorphous phase, and ionic domain. However, at high strains, network B can no longer bear the stress due to the molecular relaxation and/or crystallite disintegration, and the rubber-like network A starts to dominate. This results in the strain hardening behavior, which can be explained by deformation, reorientation, and tightening of entangled chain molecules. In Fig. 7, the results showed that at the same temperature but different RH (25 °C 50% and 80%), the mechanical behavior of the rubber-like network A does not show discernable difference, but the whole curve for network B is shifted downward as the RH increases, which indicates that the water vapor weakens the network B component more

Table 3
T and RH dependent material parameters used for FEM simulation of vapor-equilibrated membranes.

	25 °C, 50%RH	25 °C, 80%RH	65 °C, 75%RH
τ_{base}	μ_B*1.42	μ_B*1.42	μ_B*3
s_{0A}	0.75	0.8	1
s_{0B}	0.0256	0.0384	0.033

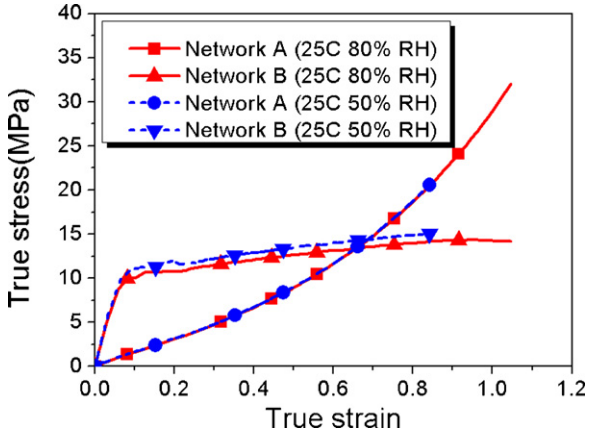

Fig. 7. Comparison of contribution of each stress components for viscoelastic network A and B from FEM simulation results for N111 at 25 °C, 50% and 80%RH.

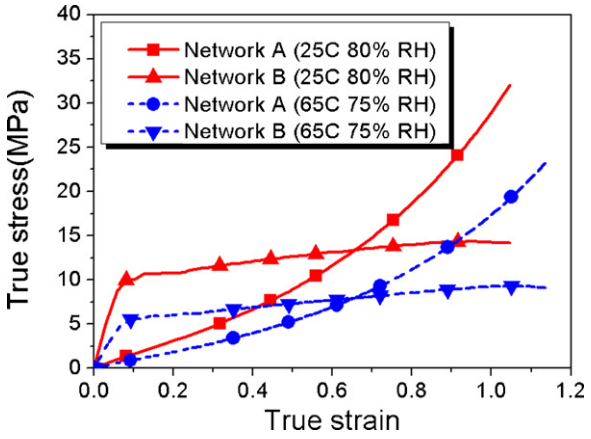

Fig. 8. Contribution of each stress components of viscoelastic network A and B from FEM simulation results for N111 at 25 °C, 80%RH and 65 °C, 75%RH.

than network A. This, in turn, imply that the water vapor interferes with intermolecular network such as secondary interaction of PTFE backbone and strong ionic interaction in the hydrophilic domain, and deteriorates their interactions [53]. However, as shown in Fig. 8, the temperature appears to influences critically on both mechanical behavior of network A and B at the same RH and reduces load-carrying capability of membranes by softening intermolecular interactions and enhancing the chain mobility in the material. There has been recent attempt to interpret the mechanical behavior by microstructure transition [5,9] due to the temperature and water activity, and it is reported that the combined effects of temperature and water alter the structure of the hydrophilic domains changing the number, strength and flexibility of cross-links between domains. The attractive interactions between sulfonic acid groups are likely to induce ionic group aggregation, which form effective cross-links that stiffen membrane at the low temperature. However, increase of temperature causes the sulfonic acid groups to become randomly dispersed and thus breaks these cross-links. The mechanical behavior predicted by our FEM analysis is consistent with these hypotheses.

In order to evaluate the effectiveness of the proposed constitutive model, water-equilibrated Nafion samples at 80 °C were tested and the stress–strain curves from the uniaxial tests were used to fit the model. In addition to that, two different strain rates of 0.3 s^{-1} and 0.0045 s^{-1} were used to verify that the model can capture the rate-dependent mechanical behavior of the ionomer membrane. Elastic modulus of water-equilibrated membrane, E, was determined from the linear curve fit to the experimental results measured from the uniaxial tension test. The material parameters are listed in Tables 4 and 5, and the results of the stress–strain

Table 4
Material parameters used in the FEM simulation of water-equilibrated membranes at 80 °C.

C	−0.5
m	6
n	4.5
β	0.6
$\dot{\gamma}_0$	1
b	0.78
ε_0	0.01
s_{0A}	2.1
s_B	4
θ_{base}	100
κ	97 MPa
λ_{lock}	6
E	25 MPa

Table 5
Strain-rate dependent material parameters used in the FEM simulation of water-equilibrated membranes at 80 °C.

	Strain rate, 0.3	Strain rate, 0.0045
τ_{base}	μ_B*2	μ_B*2.52
a	0.1	0.2
σ_0	5 MPa	3 MPa
s_{0B}	0.077	0.0625

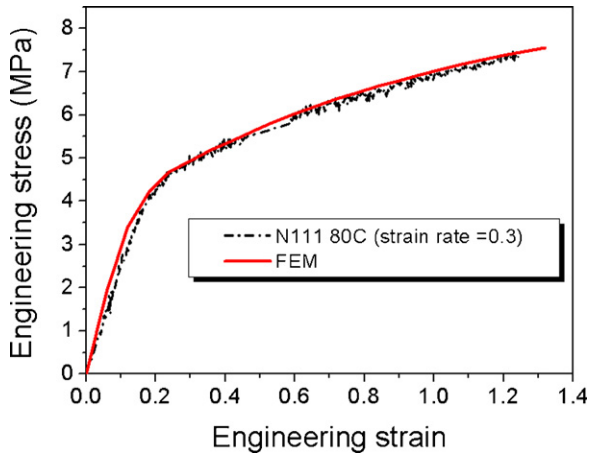

Fig. 9. Comparison the experimental data from uniaxial tension test with FEM results (a) at the strain rate 0.3 s^{-1} and (b) the strain rate 0.0045 s^{-1} under the water at 80 °C.

curves are plotted in Fig. 9. The simulated stress–strain curves show that the model can predict the rate-dependence of the mechanical behavior as expected. The true stress components of network A and B at the two different strain rate are plotted in Fig. 10, showing that high strain rate stiffens both the time-dependent network A and B.

Finally, the stress acting on each component A and B are mainly determined by the magnitude of initial shear modulus μ_A which is hypothetically related to the rubber-like network such as the molecular chain entanglement in amorphous phase of ionomer membrane and is responsible for the hardening behavior, and μ_B being associated with intermolecular interaction including ionic clusters, polymer backbone, and side chains. It is observed that s_{0A}, a ratio of μ_A and μ_B is less than unity for the FEM analysis

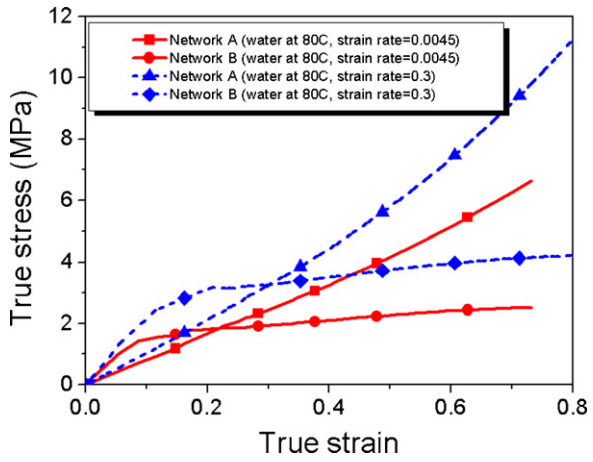

Fig. 10. Stress components from viscoelastic network A and B as revealed by the FEM simulation results for N111 at 80 °C under the water at strain rate of 0.3 s^{-1} and 0.0045 s^{-1}.

of the vapor-equilibrated membrane indicating that there is initial stiff response before the viscous flow effects dominates the behavior. The magnitude of μ_A is found to be almost two times greater than that of μ_B for the analysis of membrane immersed in a liquid water. Furthermore, the true strain at which the true stress components from network A and B intersect is approximately 0.7 for the vapor equilibrated membranes as can be seen in Figs. 7 and 8. However, the intersection point for the water equilibrated membranes is shifted down to a value less than 0.3. These observations suggest that liquid water considerably deteriorates interactions in the hydrophilic domains and any secondary interactions which might be present in the crystalline and amorphous phase being responsible for initial stiffness, and mechanical behavior of the water equilibrated membrane exhibits more likely the behavior of elastomeric materials, hence rubber-like behavior start dominates the stress–strain response at a much smaller strain than that of the vapor-equilibrated membranes.

6. Conclusion

We have developed a new constitutive model describing the finite deformation of the ionomer membrane for PEMFCs. The constitutive relationship is nonlinear viscoelastic–viscoplastic, and strain-rate, temperature, and hydration dependent. Micromechanism-inspired Bergström–Boyce model was employed to capture the nonlinear viscoelastic behavior of the membrane and reptational dynamics inspired flow rule for viscous flow was used to describe the time dependent plastic behavior. The proposed model can describe the stress–strain behavior of both vapor- and liquid-water-equilibrated membranes, and rate-dependent mechanical behavior. The simulated stress from FEM analysis is obtained from summation of two different molecular networks acting in parallel. Network A produces strain-hardening/stiffening behavior resulting from molecular reorientation, entanglement, and locking up due to the large deformation and the network B generates the initially stiff response as well as the rate, temperature, and hydration dependence of initial flow. It was found that water softens the network B component and temperature affects significantly the material behavior of both network components.

By choosing the appropriate material parameters, this model can accurately capture the mechanical behavior of ionomer over a wide range of temperature and hydration level, implying that the hypothesized mechanisms govern the material behavior of ionomer membrane. Future work is needed to improve the constitutive model by incorporating the volumetric expansion as function of hydration level into the kinematic equation, and predicting the stress and strain responses of membranes subjected to complex loading conditions and history, such as multi-axial stress in constrained membrane during dry out. As indicated earlier, we have assumed the water content and temperature in the membrane remain constant in the deformation process. The authors realize that this is an idealized situation. In reality, due to the non-linear interactions between the membrane and water, the membrane may not come to complete equilibrium with water during the deformation process. In a fuel cell, the ionomer membrane is constantly adjusting itself (deformation is one aspect of such adjustment) to equilibrate with typically non-uniform and time-varying liquid-vapor mixture of water. It takes finite time for water to be transported in or out of the membrane, in transient operation conditions membrane may not be able to come into fully equilibrated state during the deformation process. Coupled water transport and mechanical deformation models are necessary to accurately the time-dependent water-stress–strain state in the ionomers membrane.

References

[1] A. Kusoglu, A.M. Karlsson, M.H. Santare, S. Cleghorn, W.B. Johnson, Journal of Power Sources 161 (2006) 987–996.
[2] Y. Tang, A.M. Karlsson, M.H. Santara, M. Gilbert, S. Cleghorn, W.B. Johnson, An experimental investigation of humidity and temperature effects on the mechanical properties of perfluorosulfonic acid membrane, Materials Science and Engineering A 425 (2006) 297–304.
[3] P.W. Majsztrik, A.B. Bocarsly, J.B. Benziger, Review of Scientific Instruments 78 (2007) 103904.
[4] R. Solasi, Y. Zou, X. Huang, K.L. Reifsnider, D. Condit, Journal of Power Sources 167 (2008) 366–377.
[5] P.W. Majsztrik, A.B. Bocarsly, J.B. Benziger, Macromolecules 41 (24) (2008) 9849–9862.
[6] D. Bograchev, M. Gueguen, J.-C. Grandidier, S. Martemianov, Journal of Power Sources 180 (2008) 393–401.
[7] D. Bograchev, M. Gueguen, J.-C. Grandidier, S. Martemianov, International Journal of Hydrogen Energy 33 (2008) 5703–5717.
[8] F. Bauer, S. Denneler, M. Willert-Porada, Journal of Polymer Science. Part B. Polymer Physics 43 (2005) 786–795.
[9] M.B. Satterfield, J.B. Benziger, Journal of Polymer Science: Part B 47 (2009) 11–24.
[10] W. Yoon, X. Huang, Acceleration of chemical degradation of perfluorosulfonic acid ionomer membrane by mechanical stress: experimental evidence, ECS Transactions 33 (1) (2010) 907–911.
[11] W. Yoon, X. Huang, Journal of the Electrochemical Society 157 (4) (2010) B599–B606.
[12] H.E.H. Meijer, L.E. Govaert, Progress in Polymer Science 30 (2005) 915–938.
[13] M. Rubinstein, R. Colby, Polymer Physics (Oxford), 2003.
[14] D.E. Curtin, R.D. Lousenberg, T.J. Henry, P.C. Tangeman, M.E. Tisack, Journal of Power Sources 131 (2004) 41–48.
[15] K.K.R. Mocherla, Stress–strain behavior of oriented crystalline polymers: a molecular approach by dynamic infrared techniques, Ph.D. Dissertation, Material Science and Engineering Department, University of Utah, (1976).
[16] R. Solasi, Mechanical behavior, modeling, strength and failure analysis of polyelectrolyte membranes, PhD Dessertation, Mechanical Engineering Department, University of Connecticut, (2008).
[17] K. Schmidt-Rohr, Q. Chen, Nature Materials 7 (2008) 75–83.
[18] T.D. Gierke, G.E. Munn, F.C. Wilson, Journal of Polymer Science: Polymer Physics Edition 19 (11) (1981) 1687–1704.
[19] R.N. Haward, G. Thackray, Proceedings of the Royal Society of London. Series A 302 (1471) (1968) 453–472.
[20] J.S. Bergstrom, M.C. Boyce, Journal of the Mechanics and Physics of Solids 46 (5) (1998) 931–954.
[21] V.S. Kuksenko, V.P. Tamuzs, Fracture Micromechanics of Polymer Materials, Martinus Nijhoff, 1981.
[22] H.H. Kausch, Polymer Fracture, Springer-Verlag, Berlin, Heidelberg, 1987.
[23] Y. Tang, M.H. Santare, A.M. Karlsson, S. Cleghorn, W.B. Johnson, Journal of Fuel Cell Science and Technology, ASME 3 (2006) 119–124.
[24] R. Solasi, Y. Zou, X. Huang, K. Reifsnider, Mechanics of Time-Dependent Materials 12 (2008) 15–30.
[25] X. Huang, R. Solasi, Y. Zou, M. Feshler, K. Reifsnider, D. Condit, S. Burlatsky, T. Madden, Journal of Polymer Science: Part B 44 (2006) 2346–2357.
[26] E.M. Arruda, M.C. Boyce, Journal of Mechanics and Physics of Solids 41 (2) (1993) 389–412.
[27] E.M. Arruda, M.C. Boyce, R. Jayachandran, Mechanics of Materials 19 (1995) 1212–1993.
[28] S. Raha, P.B. Bowden, Polymer 13 (4) (1972) 174–183.
[29] R.P. Wool, Macromolecules 26 (1993) 1564–1569.
[30] P.G. de Gennes, Scaling Concepts in Polymer Physics, Cornell University Press, 1979.
[31] M. Doi, S.F. Edwards, The Theory of Polymer Dynamics, Oxford University Press New York, 1986.
[32] F.M. Capaldi, M.C. Boyce, Physical Review Letters 89 (17) (2002) 175505.
[33] S.F. Trevino, S.K. Young. Morphology and morphological changes within nafion membranes induced by mechanical orientation. Army Research Laboratory Report, 2002.
[34] V. Barbi, S.S. Funari, R. Gehrke, N. Scharnagl, N. Stribeck, Polymer 44 (2003) 4853–4861.
[35] J.S. Bergstrom, L.B. Hilbert Jr., Mechanics of Materials 37 (2005) 899–913.
[36] M.C. Boyce, S. Socrate, P.G. Llana, Polymer 2000 (41) (2000).
[37] J.S. Bergstrom, M.C. Boyce, Mechanics of Materials 32 (2000) 627–644.
[38] J.S. Bergstrom, S.M. Kurtz, C.M. Rimnac, A.A. Edidin, Biomaterials 23 (2002) 2329–2343.
[39] J.S. Bergstrom, Large Strain Time-Dependent Behavior of Elastomeric Materials, MIT, 1999.
[40] E.H. Lee, Journal of Applied Mechanics 36 (1969) 1–6.
[41] B. Moran, M. Ortiz, C.F. Shih, International Journal of Numerical Methods in Engineering 29 (1990) 483–514.
[42] J.A.W. Dommelen, D.M. Parks, M.C. Boyce, W.A.M. Brekelmans, F.P.T. Baaijens, Journal of the Mechanics and Physics of Solids 51 (2003) 519–541.
[43] L. Anand, M.E. Gurtin, International Journal of Solids and Structures 40 (2003) 1465–1487.
[44] M.E. Gurtin, L. Anand, International Journal of Plasticity 21 (2005) 1686–1719.
[45] A.S. Khan, H. Sujian, Continuum Theory of Plasticity, John Wiley & Sons, 1995.

[46] M.C. Boyce, G.G. Weber, D.M. Parks, Journal of the Mechanics and Physics of Solids 37 (5) (1989) 647–665.
[47] W.Y. Hsu, T.D. Gierke, Macromolecules 15 (1982) 101–105.
[48] Y. Zou, Hydrothermal mechanical properties and durability of ionomer mem branes, Master Thesis, Mechanical Engineering Department, University of Connecticut, (2007).
[49] T.E. Springer, T.A. Zawodzinski, S. Gottesfeld, Journal of Electrochemical Society 138 (8) (1991) 2334–2342.
[50] P. Areias, K. Matous, Computational Methods of Applied Mechanical Engineering 197 (2008) 4702–4717.
[51] DuPont. Nafion PFSA Membranes NRE211 and NRE-212 Product information.
[52] C. Miehe, S. Goktepe, J.M. Diez, International Journal of Solids and Structures 46 (2009) 181–202.
[53] S. Kundu, L.C. Simon, M. Fowler, S. Grot, Polymer 46 (2005) 11707–11715.